Natural abundance ^{15}N NMR by Dynamic Nuclear Polarization: Fast Analysis of Binding Sites of a novel Amine-Carboxyl-linked Immobilized Dirhodium Catalyst

Torsten Gutmann,[1#]* Jiquan Liu,[1#] Niels Rothermel,[1] Yeping Xu,[1] Eva Jaumann,[1] Mayke Werner,[1] Hergen Breitzke,[1] Snorri Th. Sigurdsson,[2] Gerd Buntkowsky[1]*

[1] *Institute of Physical Chemistry, Technical University Darmstadt, Alarich-Weiss-Straße 8, D-64287 Darmstadt, German*

* *Corresponding authors: e-mail: gutmann@chemie.tu-darmstadt.de, gerd.buntkowsky@chemie.tu-darmstadt.de*

[2] *University of Iceland, Department of Chemistry, Science Institute, Dunhagi 3, IS-107 Reykjavík, Island*

[#] These authors contributed equally to this work.

Abstract

The synthesis of a novel heterogeneous dirhodium catalyst is described. This stable catalyst is built by the dirhodium-acetate dimer (Rh_2ac_4) which is covalently linked to amine and carboxyl bifunctionalized mesoporous silica (SBA-15~NH_2~COOH). It shows good efficiency in the cyclopropanation reaction of styrene and ethyl diazoacetate (EDA) forming *cis*- and *trans*-1-ethoxycarbonyl-2-phenylcyclopropane. To characterize the structure of this catalyst and to confirm the successful immobilization heteronuclear solid-state NMR experiments are performed. The high application potential of dynamic nuclear polarization (DNP) NMR for the analysis of binding sites in this novel catalyst is demonstrated. Signal enhanced ^{13}C CP MAS and ^{15}N CP MAS techniques are employed to detect different carboxyl and amine binding sites in natural abundance at a fast time scale. The interpretation of the experimental chemical shift values for different binding sites is corroborated by quantum chemical calculations on dirhodium model complexes.

Keywords:
Dynamic Nuclear Polarization; Nuclear Magnetic Resonance; Immobilized Catalyst; Heterogeneous Catalysis; Hyperpolarization

Introduction

Dirhodium(II)-complexes are a group of multi-nuclear compounds, possessing structures containing a Rh-Rh bond and four bridging ligand moieties at equatorial positions (Fig. 1a). Such complexes were successfully applied as highly efficient catalysts in organic chemistry to produce intermediates in drug synthesis by formation of carbon-carbon or carbon-heteroatom bonds via the generation of metallo-carbenes. [1, 2] However, their technical application potential is limited by recycling and recovering problems, and especially by the strict legislation concerning metal contaminations in pharmaceutical ingredients. Aiming at a more sustainable chemistry, extensive investigations towards the development of recyclable heterogeneous dirhodium catalysts have been performed.[3] One technique to prepare heterogeneous catalysts is the immobilization of the dirhodium complex by covalent grafting employing functionalized silica or polymer materials as supporting materials. Various studies have focused on the

heterogenization on axial coordination sites (Fig. 1b) via amine or pyridine linkers which yield an efficient way to anchor different dirhodium complexes as for example chiral ones. [3-8] For the alternative heterogenization via ligand exchange (Fig. 1c) only few examples are known. In this case, at least one ligand of the original homogeneous dirhodium complex is exchanged with the carboxyl group of the functionalized silica or polymer. [9-11]

In the last decade, many types of silica based transition metal catalysts with various functionalized groups such as phosphorous, thiol, nitrogen or oxygen containing linker molecules have been synthesized and applied in catalysis. [12-33] For a rational development of this novel type of heterogeneous catalysts, it is crucial to get detailed information on the successful immobilization and further on the binding sites to understand their catalytic behavior and potential stability in reactions. In principle this analysis can be realized by structure determination employing solid-state NMR techniques, as was shown by a series of studies which characterized the structure and binding sites of such catalysts.[34-44]

In the case of phosphorous containing functionalized materials this analysis can be performed efficiently employing solid state NMR techniques due to the 100% natural abundance, the high relative sensitivity and the large gyromagnetic ratio of ^{31}P. These favorable properties allow the application of a broad range of techniques such as the standard cross polarization (CP) experiments, J-resolved or inadequate experiments, [45-47] or special heteronuclear-correlation techniques (HETCOR) designed for structure determination of such catalysts.[48, 49]

The combination of solid state NMR with quantum chemical calculations opens unique possibilities for a detailed characterization of the binding sites on the molecular level.[50, 51]

However, if less favorable nuclei, such as ^{15}N in amine containing linkers are involved, the analysis of the binding sites becomes difficult due to the low abundance, low sensitivity and low gyromagnetic ratio of the ^{15}N nucleus. In this case selective ^{15}N isotope labeling or at least isotope enrichment of the linker is mandatory to get an appropriate signal to noise ratio within reasonable time.

Hyperpolarization techniques such as Para Hydrogen Induced Polarization (PHIP),[52-55] Spin Exchange by Optical Pumping (SEOP)[56-59] or Dynamic Nuclear Polarization (DNP) are the methods of choice to overcome sensitivity problems in functionalized materials or heterogeneous catalyst systems. [60-63]

However, up to now only few studies dealt with the detection of ^{15}N in natural abundance for analysis of heterogeneous catalysts employing DNP, [64-66] which was mainly used to enhance the signals of ^{15}N for structure determination in biologically relevant systems.[67-70]

The present work focuses on the ^{15}N and ^{13}C solid state NMR characterization of a novel dirhodium catalyst immobilized on the surface of bifunctionalized mesoporous silica employing a combination of surface enhanced DNP NMR with quantum chemical calculations to model the NMR parameters of the possible binding sites.

The article is structured as follows. After this brief introduction, the experimental and computational procedures are explained in detail. In the first part of the results and discussion section, the synthesis strategy of the heterogeneous dirhodium catalyst is announced based on the rhodium acetate dimer (Rh_2ac_4) which is immobilized on the surface of bifunctionalized (amine and carboxyl) SBA-15 type material. The main part then discusses the characterization of the materials and catalysts employing conventional and/or DNP NMR spectroscopy. The interpretation of these experimental results is then argued together with theoretical results from DFT calculations. Finally, the activity of the new heterogeneous dirhodium catalyst (**3**) is investigated for the cyclopropanation reaction of styrene and ethyl diazoacetate (EDA) forming the *cis*- and *trans*-1-ethoxycarbonyl-2-phenylcyclopropane stereoisomers.

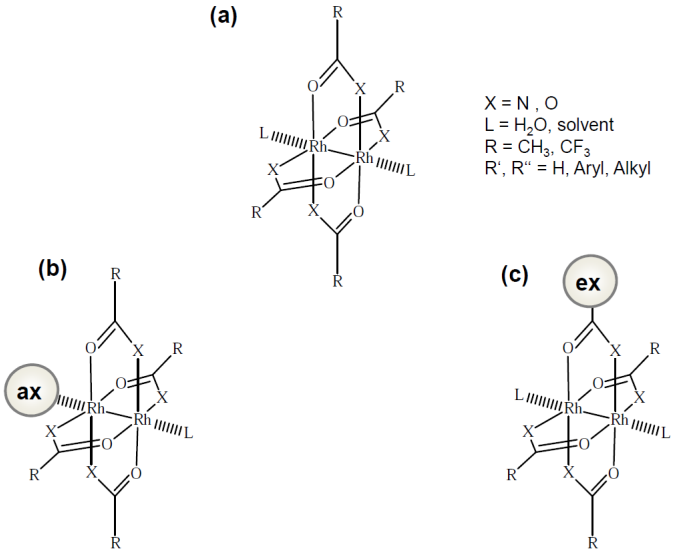

Fig. 1: (a) General structure of dirhodium(II) complexes with carboxylate or carboxamide bridging ligands. Schematic representation of binding abilities for immobilization of dirhodium(II) complexes : (b) axial coordination (**ax**), (c) ligand exchange (**ex**).

Experimental details

Preparation of the support material and immobilization of the catalyst

SBA-15~NH_2~COOH (**1**)

Bifunctionalized mesoporous silica **1** containing both amine and carboxyl groups has been synthesized by co-condensation using (3-aminopropyl)triethoxysilane (APTES, 99% wt., Sigma-Aldrich) together with carboxyethylsilanetriol sodium salt (CES, 25% vol., ABCR) following procedures given in the literature. [36, 71]

Typically, 4.0 g of Pluronic P123 (Sigma-Aldrich) as template was dissolved in 30 ml of water and 120 ml of a 2M HCl solution under stirring at 40 °C. A mixture of 6.83 g (0.0328 mol) tetraethyl orthosilicate (TEOS, 98% wt., Sigma-Aldrich), 0.91 g (0.0041 mol) APTES, 2.86 g (0.0041 mol) CES was added into the solution under stirring at 40 °C for 20 h. After aging at 80 °C for 24 h without stirring, the solid product was recovered, washed, and air-dried at room temperature. Parts of the template were removed by Soxhlet extraction with ethanol for 48 h. The obtained mesoporous silica was dried at 80 °C under vacuum to ensure total solvent removal. The maintained ordered mesoporous pores showed a narrow pore size distribution with an average diameter of 3.8 nm. The BET surface area and pore volume are calculated as 435.02 $m^2 \cdot g^{-1}$ and 0.5561 $cm^3 \cdot g^{-1}$.

Elementary analysis w%: 1.77 N, 15.30 C, 3.041 H

SBA-15~NH_2 (**2**)

Amine-functionalized mesoporous silica **2** was synthesized following the same procedure described for **1** but employing only APTES. Here a mixture of 7.69 g (0.0369mol) of TEOS and 0.91 g (0.0041mol) of APTES was utilized for the synthesis. The maintained ordered mesoporous pores showed narrow pore size distribution with an average diameter of 3.85 nm. The BET surface area and pore volume are calculated as 477.13 $m^2 \cdot g^{-1}$ and 0.5476 $cm^3 \cdot g^{-1}$.

Elementary analysis w%: 1.33 N, 4.504 C, 3.206 H

SBA-15~NH_2 ~COOH + Rh_2ac_4 (**3**)

The immobilization of the dirhodium catalyst was achieved by wet impregnation following a heating step under vacuum. 0.01 g rhodium acetate dimer was dissolved in acetonitrile. Then 1 g bifunctional mesoporous silica **1** was impregnated in such solution. After evaporation of the solvent at room temperature, small amounts of acetonitrile were added to ensure the dirhodium complex was adsorbed in mesoporous silica as much as possible. This process was repeated 5 times. Then, the air dried solid was heated at 80 ℃ under vacuum for 24 h to remove the side product (acetic acid). The catalyst was washed by Soxhlet extraction with acetonitrile for 48 h to remove physisorbed and neat dirhodium complex. Finally, the product was dried under vacuum yielding the heterogeneous catalyst as grey green powder. The obtained catalyst showed decreased BET surface area of 229.88 $m^2 \cdot g^{-1}$ and pore volume of 0.162 $cm^3 \cdot g^{-1}$.
Elementary analysis w%: 1.679 N, 12.19 C, 3.087 H

Solid-State NMR experiments without DNP

All room temperature solid-state NMR spectra were measured at a 500 MHz Varian Unity Inova spectrometer equipped with a Bruker 4 mm standard bore HX MAS. Spectra were recorded at a frequency of 125.81 MHz for ^{13}C and 99.36 MHz for ^{29}Si. Cross polarization (CP) experiments were performed with contact times of 3 ms for ^{13}C and ^{29}Si at a spinning rate of 6 kHz. Measurements take approximately one night to get an appropriate signal.

DNP enhanced Solid-State NMR experiments

For all DNP measurements 1-(TEMPO-4-oxy)-3-(TEMPO-4-amino)propan-2-ol (TOTAPOL) was employed as prominent biradicalic polarizing agent.[72] The synthesis of this radical was performed according to the procedure described by Song et al. [73] For the typical sample preparation, 15-25 mg of the functionalized material was wetted with 15 µL of a 0.015 M solution of TOTAPOL in D_2O/H_2O 90:10 and packed in 3.2 mm sapphire rotors.
All DNP enhanced solid-state NMR experiments were performed on a Bruker Avance III 400 spectrometer system equipped with an Ascend™ 400 DNP magnet, with a low-temperature triple resonance $^1H/X/Y$ probe, and a 9.7 Tesla Bruker gyrotron system corresponding to a microwave frequency of 263 GHz.
Spectra were recorded at a frequency of 400.02 MHz for ^1H, 100.59 MHz for ^{13}C and 40.53 MHz for ^{15}N to reach the optimum match with the microwave source.
^{13}C and ^{15}N spectra were measured at nominally 100 K and at 8 kHz spinning rate. Cross polarization (CP) experiments were performed with contact times of 2 ms for ^{13}C and 3 ms for ^{15}N, and a repetition delay of 10 s according to the approximated T_1 times of the protons in these samples at this temperature. 128 accumulations were performed for ^{13}C (measurement time 21 min) and 5000 accumulations were performed for ^{15}N spectra (measurement time 14 h). During data acquisition dipolar interactions to protons were decoupled employing tppm decoupling[74] with a 20° phase jump. All ^{13}C spectra were referenced to TMS and ^{15}N spectra were referenced to CH_3NO_2 employing NH_4Cl as external standard (-341.168 ppm[75]).

Activity test of the heterogeneous dirhodium catalyst

To test the activity of the SBA-15~NH_2~COOH+Rh_2ac_4 (**3**) catalyst the cyclopropanation of ethyl diazoacetate (EDA) and styrene was investigated as model reaction.[7] In a typical procedure 1.04 g styrene was added to a suspension of 0.075 g of the catalyst in 6.65 g CH_2Cl_2, and the mixture was treated with ultrasonic dispersion for 15 min. Then 0.058 g EDA in 2 g CH_2Cl_2 was added and the mixture was stirred at room temperature. Samples were taken after 15 min, 1 h, 2 h, 3 h, 4 h and 5 h and analyzed by gas chromatography (GC) (Agilent Technologies 7820A), which was equipped with a HP-5 (30m × 0.32mm × 0.25µm) column and a FID detector. For separation of the stereoisomers a GC temperature program was chosen

starting from 80°C with an 8°C/min ramp for 3 min followed by a 15°C/min ramp for 8 min at a N_2 gas flow of 1.4 mL/min. Thus, the retention times for the *cis*- and the *trans*-isomer were 8.2 min and 8.6 min, respectively.

Computational details

All DFT calculations were carried out with the Orca program system.[76] Model structures for the coordination of amine-linkers to Rh_2ac_4 were created from the crystal structure of $Rh_2(Ac)_4(H_2O)_2$ [77] replacing one (structure **I**) respectively two (structure **II**) of the water molecules by propylamine. Geometry optimization was performed with Becke's three-parameter hybrid functional [78, 79] along with the Lee-Yang-Parr correlation functional (B3LYP), [80] and Pople's double-ζ basis set 6-31G(d,p) combining d- and p-polarization functions. [81, 82] In these optimization runs the core electrons for Rh were replaced by the fully relativistic effective core potential (ECP) developed by the Stuttgart group. [83]
Calculations of ^{15}N chemical shieldings were performed at the same level of theory employing the triple-ζ basis set 6-311++G(3df,3dp) including four sets of polarization functions and additional diffuse functions on all atoms. [81, 82, 84-86]
For easier assignment of the ^{13}C signals of the supporting material SBA-15~NH_2~COOH (**1**) chemical shift predictions based on atomic increment algorithms were arranged employing the ACD Labs software package.

Results and Discussion

Synthesis and basic characterization of the immobilized dirhodium catalyst

Before starting the immobilization of the homogeneous dirhodium catalyst the bifunctionalized supporting material SBA-15~NH_2~COOH (**1**) was synthesized. This synthesis procedure followed a slightly modified version of the co-condensation[36] to achieve a relatively homogeneous distribution of carboxyl and amine groups on the surface of the mesoporous material. According to the N_2 adsorption–desorption isotherms of the support material (see ESI S0a), the type IV isotherm with H1 hysteresis in the mesopore range demonstrate the presence of open-ended cylindrical mesopores, which is a feature of an SBA-15 type mesoporous matrix. This supporting material was then used to graft the homogeneous dirhodium complex in two steps. In the wet impregnation step which was performed at room temperature the Lewis acidic dirhodium complex is forced to form an axial coordination site with the amine group.[7] In the heating step under vacuum, the carboxyl groups on the surface of the mesoporous silica favor ligand exchange with the dirhodium complex. Following this synthesis protocol, it can be assumed that the dirhodium complex is attached to the surface via both, the amine and the carboxyl functions. The immobilized catalyst displays a type IV isotherm but in contrary to the supporting material with H3 hysteresis (see ESI S0b). The pore size distribution became broader and the average diameter of the pore has decreased. This is a further hint that the dirhodium complex has dropped in the mesopores after immobilization.

Solid-State NMR Characterization

^{29}Si solid-state NMR

To characterize the surface of the SBA-15~NH_2~COOH (**1**) supporting material, ^{29}Si CP-MAS NMR spectra were recorded (Fig. 2). The three signals at -99, -106 and -114 ppm are assigned to the silicon atoms of silanol groups labeled as Q2, Q3, and Q4 which are present on the surface. [34, 36, 87] Structural changes of the silica surface due to the binding of amine and carboxyl-linkers are revealed by appearance of T_n signals (-66 ppm and -72 ppm). These signals result from the reaction of the APTES and CES-linker with TEOS during the co-condensation process forming one, two or three -Si-O-Si- bonds. This confirms the successful functionalization of the surface which is achieved via covalent binding. Interestingly, in contrast to the previously published data for SiO_2 nanoparticles[87] or functionalized SBA-3 material [34] only two resolvable signals are observed. We assume that this phenomenon results from the co-condensation method employed for the preparation.

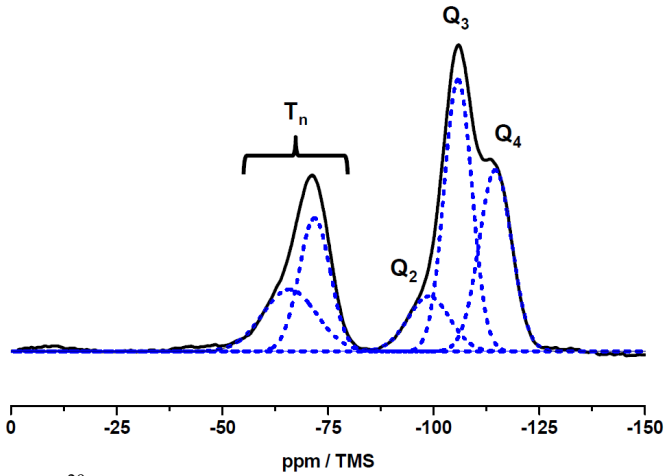

Fig. 2 ^{29}Si CP MAS spectrum of the bi-functionalized SBA-15~NH_2 ~COOH (**1**) material at 6 kHz spinning. The observation of T_n - groups confirms the successful functionalization of the SBA-15 material.

After immobilization of the Rh_2ac_4 catalyst, the ^{29}Si CP-MAS spectrum (see ESI S1) did not noticeable change as already observed for the Wilkinson's catalyst immobilized on functionalized SBA-3 material.[34] This shows on the one hand that the rhodium has no significant influence on the chemical environment of the silica, and further proves the stability of the material which is not influenced by the metal.

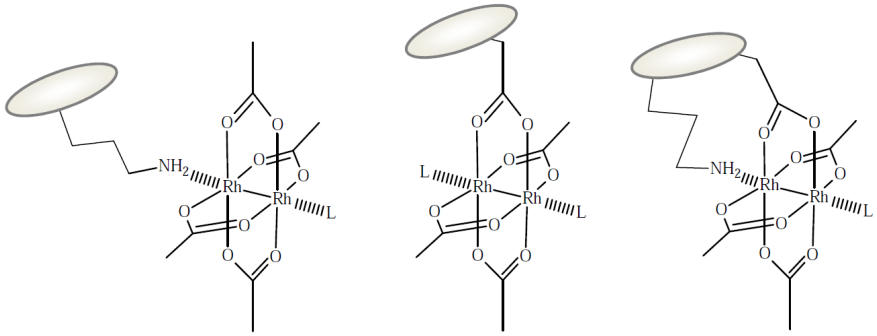

Fig. 3 Possible binding configurations for the immobilization of Rh_2ac_4: (a) axial coordination via amine , (b) ligand exchange with the carboxylate group, and (c) coordination via amine and ligand exchange with the carboxylate group.

^{13}C solid state DNP NMR

Fig. 4a shows the ^{13}C spectrum of the supporting material **1** recorded with microwave irradiation. From this spectrum it is evident that the SBA-15 material contains two different types of linker molecules namely the CES linker represented by the characteristic chemical shift of the CO group in the range of 180 ppm and two signals in the aliphatic region, and the APTES linker represented by three signals in the aliphatic region. From the prediction of ^{13}C NMR chemical shifts by atomic increment based algorithms, one can assume that the signals at 8.9 ppm, 21.1 ppm and 42.2 ppm assign to the APTES linker while the signals at 13.8 ppm and 29.5 ppm assign to the CES linker. Interestingly, the broad signal at 180 ppm consists of two overlapping signals (Fig. 4a, details), one at 183.3 ppm and a second one at 178.0 ppm. This observation is a first hint that next to the carboxyl function expected at 183.3 ppm the sample also consists of a carbamide function where the ^{13}C signal is highfield shifted to 178.0 ppm. Next to these signals, a signal group centered at 70 ppm is visible which refers to template molecules which were not completely removed during the synthesis.

After immobilization of the Rh_2ac_4 the ^{13}C CP MAS spectrum changed and additional small overlapping signals in the aliphatic region appear (Fig. 4b). They assign the acetate ligand system of Rh_2ac_4. In the region of CO groups, a third overlayed signal appears (Fig. 4b, details) at 190.5 ppm which clearly indicates carbonyl functions coordinating the dirhodium. A similar chemical shift is also found for the neat crystalline Rh_2ac_4 catalyst (see ESI S2) however the line-width for the neat catalyst (ca. 550 Hz) is smaller than for the immobilized catalyst (ca. 820 Hz). This is a strong indication that the catalyst is bound after exchange of an acetate ligand via the carbonyl-function as displayed in Fig. 3b. Since excess of the neat catalyst as well as physisorbed Rh_2ac_4 were removed from the surface by washing with acetonitrile, the new signal at 190.5 ppm clearly assigns the chemically bound catalyst on the surface.

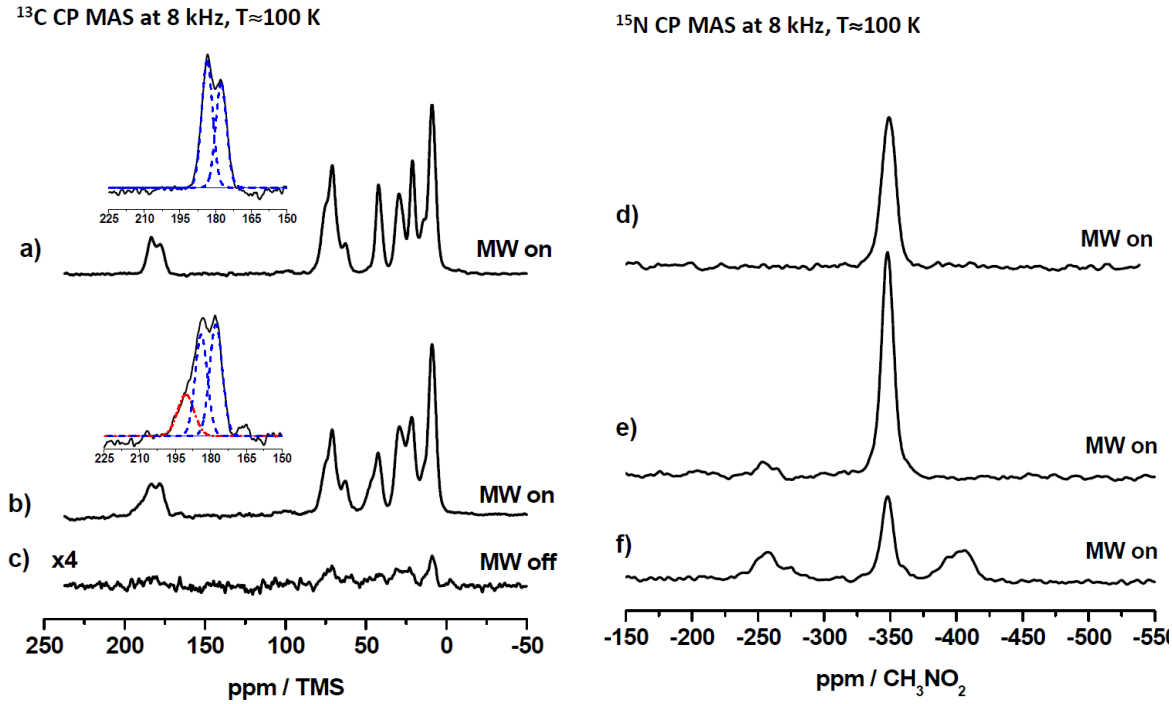

Fig. 4 ^{13}C and ^{15}N NMR spectra measured at 8 kHz spinning at nominally 100 K: (a) ^{13}C CP MAS of SBA-15~NH_2~COOH (**1**) with MW on and deconvolution of the signals of the carbonyl functions, (b) ^{13}C CP MAS of SBA-15~NH_2 ~COOH + Rh_2ac_4 (**3**) with MW on and deconvolution of the signals of the carbonyl functions, (c) ^{13}C CP MAS of SBA-15~NH_2~COOH + Rh_2ac_4 (**3**) with MW off, (d) ^{15}N CP MAS of SBA-15~NH_2 (**2**) with MW on, (e) ^{15}N CP MAS of SBA-15~NH_2~COOH (**1**) with MW on, and (f) ^{15}N CP MAS of SBA-15~NH_2~COOH + Rh_2ac_4 (**3**) with MW on.

^{15}N solid state DNP NMR

While the sensitivity of ^{13}C CP MAS spectroscopy is in principle high enough to record the natural abundance ^{13}C spectra employing long measurement times and signal averaging, this is not feasible for natural abundance ^{15}N CP MAS, since it is roughly two orders of magnitude less sensitive. Here, the sensitivity is limited by the low natural abundance (0.368%) and the low gyromagnetic ratio ^{15}N ($-2.7126 \cdot 10^7$ rad $T^{-1}s^{-1}$) of the ^{15}N nucleus. Thus, for standard solid-state NMR isotope labeling with ^{15}N would be required which cannot be realized with typical synthetic strategies for the investigated systems.

The ^{15}N CP MAS spectra measured with DNP (see Fig. 4d-f) overcome these sensitivity problems. All spectra were recorded within 14 h of measurement time with an appropriate S/N ratio which allows clear assignment of signals. Fig. 4d shows the spectrum of pure amino-functionalized SBA-15 material (**2**). The broad signal at -349.0 ppm refers to free amine functions which build up a large distribution of isotropic chemical shifts due to various chemical environments in the amorphous sample. When functionalizing the SBA-15 material with additional carboxyl-linkers (**1**) the spectral line-shape slightly changes and a second signal located at approximately -258 ppm appears. Together with the signal at 178 ppm in the ^{13}C spectrum (see above) this second signal clearly demonstrates the existence of carbamide on the surface of the supporting material which may result from a condensation of amine and carboxyl function on the surface of the SBA-type material, or by reaction of amine function with atmospheric carbon-dioxide as investigated by Shimming et al.[88]

After immobilization of Rh_2ac_4 on **1** the intensity of the signal at -349.0 ppm decreased and a new signal at -402.7 ppm appeared. Such observation is a strong hint that the rhodium of the neat Rh_2ac_4 catalyst coordinates at the amine function of **1** in a way illustrated in Fig. 3a or Fig. 3c.

Quantum Chemical calculations

To support the assignment of the ^{15}N signals in the solid-state spectra theoretical calculations were performed on model systems of Rh_2ac_4. N-propylamine (**III**) was chosen as model ligand to simulate the coordination of the dirhodium complex to silica that was functionalized with APTES. Since we aimed on isotropic chemical shift information, it is reasonable to dismiss the silica part of the system in favor of computational costs. In addition to that, the theoretical results can be easily compared to the previous liquid state NMR data.

Two different structures (see Fig. 5) were created replacing one (structure **I**) or two (structure **II**) of the water ligands by n-propylamine which model the most probable coordination sites of amine to Rh_2ac_4.

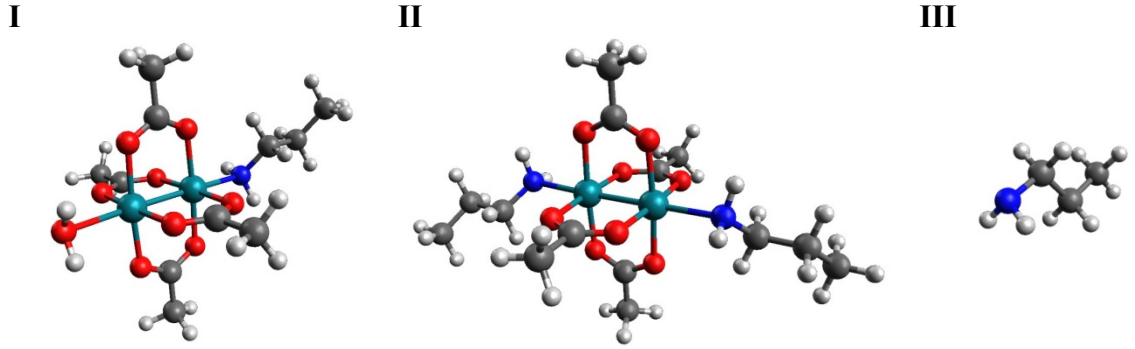

Fig. 5 Structures for the NMR parameter calculations: n-propylamine monosubstituted dirhodium complex (**I**), n-propylamine disubstituted dirhodium complex (**II**) and n-propylamine (**III**).

In Table 1 the chemical shifts (referenced to CH_3NO_2) calculated for the nitrogen nuclei in the three displayed structures are summarized. Comparing the shifts of the free amine group (structure **III**) with the rhodium bound amine groups in structure **I** the highfield shift of approximately 35.8 ppm observed in the liquid spectrum (see ESI S3) is confirmed in excellent agreement.

The calculated difference between the single amine coordination in structure **I** and the double coordination in structure **II** (10 ppm) is relatively small and does not allow a clear discrimination between these two possibilities of coordination within the error margins of the employed B3LYP/6-311++G(3df,3dp) level of theory.

For the interpretation of the chemical shifts observed in the solid-state spectra, the calculated ^{15}N values for the amine groups can only give a hint on the change of electronic structure when coordinating at rhodium. The calculated highfield shift of 35.8 ppm is also present in the solid-state spectrum but with stronger characteristic (53.7 ppm).

These results strongly fortify the hypothesis that the homogeneous dirhodium catalyst is immobilized via one amine linker.

Structure	$\delta^{15}N$ calculated (ppm/CH_3NO_2)	$\delta^{15}N$ experimental liquid state NMR (ppm/CH_3NO_2)	$\delta^{15}N$ experimental solid state NMR (ppm/ CH_3NO_2)
I	-397.5	-395.7	-402.7
II	-387.4/-388.3		
III	-363.2	-359.9	-349.0

Table 1: Calculated ^{15}N chemical shifts of structures **I** –**III** and comparison with experimental ^{15}N chemical shifts from liquid state and solid state NMR.

Sensitivity enhancement by DNP

To illustrate the efficiency of the DNP enhanced solid-state NMR approach a ^{13}C reference spectrum for SBA-15~NH_2~COOH + Rh_2ac_4 (**3**) was recorded employing the same parameters but without microwave irradiation (Fig. 4c). This spectrum shows no significant signals within the applied measurement time of 20 min. Compared to this spectrum, the S/N ratio of the DNP spectrum is improved by a factor of 24. This enhancement factor is comparable to the values reached by other groups for surface enhanced DNP on functionalized porous silica materials. [89] For ^{15}N the enhancement factor was only calculated for the SBA-15~NH_2 (**2**) (see ESI S4) which served as test sample for evaluation of the^{15}N DNP setup. Even without any optimizations an enhancement factor of about 6 was achieved, which corresponds in a time gain of 36, compared to the standard solid state NMR experiment. This demonstrates clearly the high potential of the ^{15}N DNP to characterize nitrogen containing binding sites in heterogeneous systems.

Activity test of the SBA-15~NH_2~COOH+Rh_2ac_4 (3) catalyst

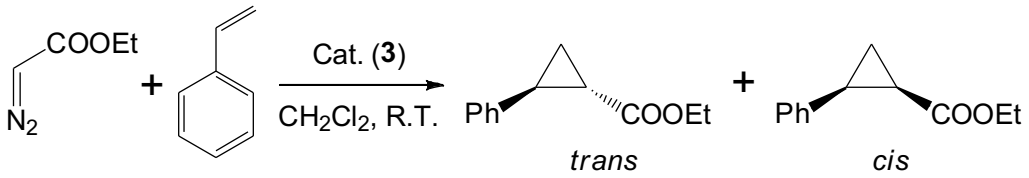

Scheme 1: Reaction scheme of the cyclopropanation of EDA with styrene according to ref. [7] catalyzed by SBA-15~NH_2~COOH + Rh_2ac_4 (**3**).

To test the catalytic application potential of the heterogeneous dirhodium catalyst (**3**) a model cyclopropanation reaction was performed employing EDA and styrene as substrates (Scheme 1). The results of this activity study are graphically displayed in Fig. 6. The overall yield of the products (*cis*- and *trans*-1-ethoxycarbonyl-2-phenylcyclopropane) increased with the reaction time and reached about 55% after 5 hours. During the reaction, the percentage of the *cis*-isomer in the products kept at 45% and for the *trans*-isomer at 55% showing that both products can be produced with good yields. This confirms the efficiency of the heterogeneous dirhodium catalyst towards cyclopropanation even without optimization of the catalyst structure and demonstrates the application potential of this catalyst for preparing precursors for pharmaceutical ingredients.

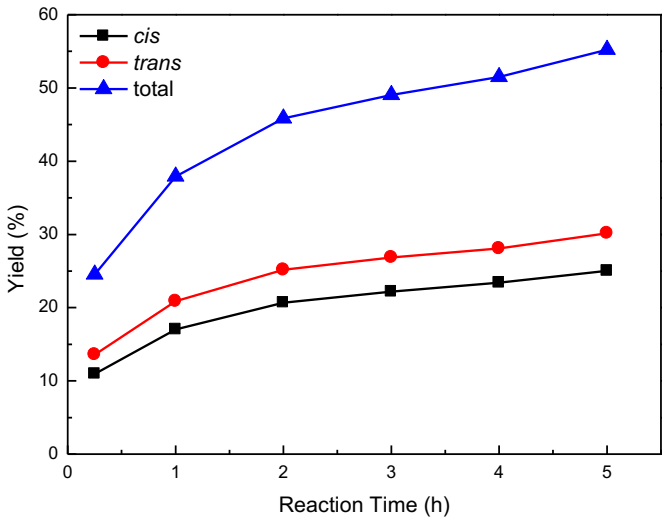

Fig. 6 Overall yield of the product mixture (▲), of the *cis*- (■), and the *trans*-isomer (●) as function of the reaction time.

Conclusion

The synthesis of a novel heterogeneous dirhodium catalyst based on functionalized silica supporting material is shown. The dirhodium acetat dimer (Rh_2ac_4) is chosen as model complex which is grafted on bi-functionalized mesoporous silica (SBA-15~NH_2~COOH).

This catalyst is applied in the cylcopropanation reaction of EDA and styrene showing efficient conversion to form the *cis*- and *trans*-1-ethoxycarbonyl-2-phenylcyclopropane product at room temperature.

^{29}Si solid-state NMR demonstrates the successful functionalization of the mesoporous SBA-15 material. Surface enhanced ^{13}C CP MAS and ^{15}N CP MAS experiments allow to distinguish different binding sites on the supporting material such as carbonyl, amine and carbamide functions. Such experiments also confirm that the dirhodium catalyst is attached via an amine and/or carboxyl group to the surface. The interpretation of the chemical shift values for different binding sites is corroborated by quantum chemical calculations on dirhodium model complexes which are in excellent agreement with the experiment.

This study clearly demonstrates the high application potential of DNP NMR to detect nuclei such as ^{15}N in natural abundance which can be employed to distinguish different amine binding sites in heterogeneous catalysts systems at a fast time scale. Furthermore, it opens the possibility to analyze a wide range of systems with nitrogen containing groups that cannot be easily spin labeled.

Acknowledgement

This work has been supported by the Deutsche Forschungsgemeinschaft (DFG) under contract Bu-911-20-1 which gave us the opportunity to set-up the DNP spectrometer and Bu-911-12-2, and the Islandic Research Fund (141062-051). We further thank Bruker Biospin Germany and France for technical installation and support of the DNP spectrometer. Particular acknowledge is given to the technicians N. Mathieu, F. Rohé and F. Aussenac from Bruker France for their

excellent technical support on the DNP. We thank Dr. R. Meusinger from the organic chemistry department (TU Darmstadt) for measuring the 2D liquid-state NMR spectra.

References

1 H. M. L. Davies and R. E. J. Beckwith, *Chem. Rev.*, 2003, **103**, 2861-2903.
2 M. P. Doyle, R. Duffy, M. Ratnikov and L. Zhou, *Chem. Rev.*, 2010, **110**, 704-724.
3 N. R. Candeias, C. A. M. Afonso and P. M. P. Gois, *Org. Biomol. Chem.*, 2012, **10**, 3357-3378.
4 H. M. L. Davies and A. M. Walji, *Org. Lett.*, 2003, **5**, 479-482.
5 H. M. L. Davies and A. M. Walji, *Org. Lett.*, 2005, **7**, 2941-2944.
6 H. M. L. Davies, A. M. Walji and T. Nagashima, *J. Am. Chem. Soc.*, 2004, **126**, 4271-4280.
7 E. V. Dikarev, D. K. Kumar, A. S. Filatov, A. Anan, Y. Xie, T. Asefa and M. A. Petrukhina, *ChemCatChem*, 2010, **2**, 1461-1466.
8 T. Nagashima and H. M. L. Davies, *Org. Lett.*, 2002, **4**, 1989-1992.
9 D. E. Bergbreiter, M. Morvant and B. Chen, *Tetrahedron Lett.*, 1991, **32**, 2731-2734.
10 H. M. Hultman, M. de Lang, M. Nowotny, I. Arends, U. Hanefeld, R. A. Sheldon and T. Maschmeyer, *J. Catal.*, 2003, **217**, 264-274.
11 K. Takeda, T. Oohara, M. Anada, H. Nambu and S. Hashimoto, *Angewandte Chemie-International Edition*, 2010, **49**, 6979-6983.
12 D. Brunel, N. Bellocq, P. Sutra, A. Cauvel, M. Lasperas, P. Moreau, F. Di Renzo, A. Galarneau and F. Fajula, *Coord. Chem. Rev.*, 1998, **180**, 1085-1108.
13 P. Iliade, I. Miletto, S. Coluccia and G. Berlier, *Res. Chem. Intermed.*, 2012, **38**, 785-794.
14 X. S. Zhao, X. Y. Bao, W. Guo and F. Y. Lee, *Mater. Today*, 2006, **9**, 32-39.
15 J. O. Krause, O. Nuyken, K. Wurst and M. R. Buchmeiser, *Chemistry-a European Journal*, 2004, **10**, 777-784.
16 H. Brunner, E. Bielmeier and J. Wiehl, *J. Organomet. Chem.*, 1990, **384**, 223-241.
17 J. Evans, A. B. Zaki, M. Y. El-Sheikh and S. A. El-Safty, *J. Phys. Chem. B*, 2000, **104**, 10271-10281.
18 C. Merckle, S. Haubrich and J. Bluemel, *J. Organomet. Chem.*, 2001, **627**, 44-54.
19 H. Werner and U. Mohring, *J. Organomet. Chem.*, 1994, **475**, 277-282.
20 A. J. Sandee, J. N. H. Reek, P. C. J. Kamer and P. W. N. M. van Leeuwen, *J. Am. Chem. Soc.*, 2001, **123**, 8468-8476.
21 W. H. Cheung, W. Y. Yu, W. P. Yip, N. Y. Zhu and C. M. Che, *J. Org. Chem.*, 2002, **67**, 7716-7723.
22 H. L. Li, N. Perkas, Q. L. Li, Y. Gofer, Y. Koltypin and A. Gedanken, *Langmuir*, 2003, **19**, 10409-10413.
23 A. Crosman and W. E. Hoelderich, *J. Catal.*, 2005, **232**, 43-50.
24 C. Merckle and J. Bluemel, *Top. Catal.*, 2005, **34**, 5-15.
25 A. M. J. Rost, H. Schneider, J. P. Zoller, W. A. Herrmann and F. E. Kuhn, *J. Organomet. Chem.*, 2005, **690**, 4712-4718.
26 N. K. K. Raj, S. S. Deshpande, R. H. Ingle, T. Raja and P. Manikandan, *Stud. Surf. Sci. Catal.*, 2005, **156**, 769-778.
27 P. M. Rao, A. Wolfson, S. Kababya, S. Vega and M. V. Landau, *J. Catal.*, 2005, **232**, 210-225.
28 J. Kasai, Y. Nakagawa, S. Uchida, K. Yamaguchi and N. Mizuno, *Chemistry-a European Journal*, 2006, **12**, 4176-4184.
29 T. Posset and J. Bluemel, *J. Am. Chem. Soc.*, 2006, **128**, 8394-8395.

30 F. Hoffmann, M. Cornelius, J. Morell and M. Froba, *J. Nanosci. Nanotechnol.*, 2006, **6**, 265-288.
31 M. Heitbaum, F. Glorius and I. Escher, *Angew. Chem.- Int. Ed.*, 2006, **45**, 4732-4762.
32 T. Joseph, S. S. Deshpande, S. B. Halligudi, A. Vinu, S. Ernst and M. Hartmann, *J. Mol. Catal.*, 2003, **A 206**, 13-21.
33 S. Shylesh, S. Sharma, S. P. Mirajkar and A. P. Singh, *J. Mol. Catal.*, 2004, **212**, 219-228.
34 A. Grünberg, Y. P. Xu, H. Breitzke and G. Buntkowsky, *Chem. - Eur. J.*, 2010, **16**, 6993-6998.
35 M. Yang, F. F. Xu, C. Wang, X. M. Liu, P. F. Yan, P. P. Li and U. Welz-Biermann, *Eur. J. Inorg. Chem.*, 2012, 4500-4506.
36 M. Colilla, I. Izquierdo-Barba, S. Sánchez-Salcedo, J. L. G. Fierro, J. L. Hueso and M. Vallet-Regí, *Chem. Mater.*, 2010, **22**, 6459-6466

37 M. W. McKittrick and C. W. Jones, *J. Catal.*, 2004, **227**, 186-201.
38 J. L. Rapp, Y. Huang, M. Natella, Y. Cai, V. S. Y. Lin and M. Pruski, *Solid State Nucl. Magn. Reson.*, 2009, **35**, 82-86.
39 A. Adamczyk, Y. Xu, B. Walaszek, F. Roelofs, T. Pery, K. Pelzer, K. Philippot, B. Chaudret, H. H. Limbach, H. Breitzke and G. Buntkowsky, *Top. Catal.*, 2008, **48**, 75-83.
40 J. Bluemel, *Coord. Chem. Rev.*, 2008, **252**, 2410-2423.
41 A. Grünberg, H. Breitzke and G. Buntkowsky, *Spectroscopic Properties of Inorganic and Organometallic Compounds: Techniques, Materials and Applications*, 2012, **43**, 289-323.
42 J. Bluemel, *Nachrichten aus der Chemie*, 2006, **54**, 632-638.
43 T. Iwai, R. Tanaka, T. Harada and M. Sawamura, *Chem. - Eur. J.*, 2014, **20**, 1057-1065.
44 S. Sanchez-Salcedo, M. Colilla, I. Izquierdo-Barba and M. Vallet-Regi, *Journal of Materials Chemistry B*, 2013, **1**, 1595-1606.
45 G. Wu and R. E. Wasylishen, *Organometallics*, 1992, **11**, 3242-3248.
46 G. Wu and R. E. Wasylishen, *J. Chem. Phys.*, 1993, **98**, 6138-6149.
47 G. Wu and R. E. Wasylishen, *Inorg. Chem.*, 1996, **35**, 3113-3116.
48 K. Mao, J. W. Wiench, V. S. Y. Lin and M. Pruski, *J. Magn. Reson.*, 2009, **196**, 92-95.
49 J. W. Wiench, C. Michon, A. Ellern, P. Hazendonk, A. Iuga, R. J. Angelici and M. Pruski, *J. Am. Chem. Soc.*, 2009, **131**, 11801-11810.
50 A. Gruenberg, T. Gutmann, N. Rothermel, Y. Xu, H. Breitzke and G. Buntkowsky, *Z. Phys. Chem.*, 2013, **227**, 901-915.
51 T. Gutmann, A. Gruenberg, N. Rothermel, M. Werner, M. Srour, S. Abdulhussain, S. Tan, Y. Xu, H. Breitzke and G. Buntkowsky, *Solid State Nucl. Magn. Reson.*, 2013, **55-56**, 1-11.
52 S. S. Arzumanov and A. G. Stepanov, *J. Phys. Chem. C*, 2013, **117**, 2888-2892.
53 H. Henning, M. Dyballa, M. Scheibe, E. Klemm and M. Hunger, *Chem. Phys. Lett.*, 2013, **555**, 258-262.
54 K. V. Kovtunov, V. V. Zhivonitko, I. V. Skovpin, D. A. Barskiy and I. V. Koptyug, in *Hyperpolarization Methods in Nmr Spectroscopy*, 2013, vol. 338, pp. 123-180.
55 A. A. Lysova and I. V. Koptyug, *Chem. Soc. Rev.*, 2010, **39**, 4585-4601.
56 J. L. Bonardet, J. Fraissard, A. Gedeon and M. A. Springuel-Huet, *Catal. Rev. - Sci. Eng.*, 1999, **41**, 115-225.
57 E. Brunner, *Concepts Magn. Reson.*, 1999, **11**, 313-335.
58 W. Happer, E. Miron, S. Schaefer, D. Schreiber, W. A. van Wijngaarden and X. Zeng, *Phys. Rev. A*, 1984, **29**, 3092-3110.
59 Y. Liu, W. Zhang, X. Han and X. Bao, *Chinese Journal of Catalysis*, 2006, **27**, 827-836.

60 A. J. Rossini, A. Zagdoun, M. Lelli, A. Lesage, C. Copéret and L. Emsley, *Acc. Chem. Res.*, 2013, **46**, 1942-1951.
61 T. Maly, G. T. Debelouchina, V. S. Bajaj, K. N. Hu, C. G. Joo, M. L. Mak-Jurkauskas, J. R. Sirigiri, P. C. A. van der Wel, J. Herzfeld, R. J. Temkin and R. G. Griffin, *J. Chem. Phys.*, 2008, **128**, 052211
62 T. Kobayashi, O. Lafon, A. S. Lilly Thankamony, I. I. Slowing, K. Kandel, D. Carnevale, V. Vitzthum, H. Vezin, J.-P. Amoureux, G. Bodenhausen and M. Pruski, *Phys. Chem. Chem. Phys.*, 2013, **15**, 5553-5562.
63 U. Akbey, B. Altin, A. Linden, S. Ozcelik, M. Gradzielski and H. Oschkinat, *Phys. Chem. Chem. Phys.*, 2013, **15**, 20706-20716.
64 A. J. Rossini, A. Zagdoun, M. Lelli, J. Canivet, S. Aguado, O. Ouari, P. Tordo, M. Rosay, W. E. Maas, C. Copéret, D. Farrusseng, L. Emsley and A. Lesage, *Angewandte Chemie-International Edition*, 2012, **51**, 123-127.
65 W. R. Gruening, A. J. Rossini, A. Zagdoun, D. Gajan, A. Lesage, L. Emsley and C. Copéret, *Phys. Chem. Chem. Phys.*, 2013, **15**, 13270-13274.
66 F. Blanc, S. Y. Chong, T. O. McDonald, D. J. Adams, S. Pawsey, M. A. Caporini and A. I. Cooper, *J. Am. Chem. Soc.*, 2013, **135**, 15290−15293.
67 M. Rosay, J. C. Lansing, K. C. Haddad, W. W. Bachovchin, J. Herzfeld, R. J. Temkin and R. G. Griffin, *J. Am. Chem. Soc.*, 2003, **125**, 13626-13627.
68 G. T. Debelouchina, M. J. Bayro, P. C. A. van der Wel, M. A. Caporini, A. B. Barnes, M. Rosay, W. E. Maas and R. G. Griffin, *Phys. Chem. Chem. Phys.*, 2010, **12**, 5911-5919.
69 I. Gelis, V. Vitzthum, N. Dhimole, M. A. Caporini, A. Schedlbauer, D. Carnevale, S. R. Connell, P. Fucini and G. Bodenhausen, *J. Biomol. NMR*, 2013, **56**, 85-93.
70 V. S. Bajaj, M. L. Mak-Jurkauskas, M. Belenky, J. Herzfeld and R. G. Griffin, *J. Magn. Reson.*, 2010, **202**, 9-13.
71 I. Izquierdo-Barba, S. Sánchez-Salcedo, M. Colilla, M. J. Feito, C. Ramírez-Santillán, M. T. Portolés and M. Vallet-Regí, *Acta Biomaterialia*, 2011, **7**, 2977-2985.
72 K. N. Hu, C. Song, H. H. Yu, T. M. Swager and R. G. Griffin, *J. Chem. Phys.*, 2008, **128**, 17.
73 C. S. Song, K. N. Hu, C. G. Joo, T. M. Swager and R. G. Griffin, *J. Am. Chem. Soc.*, 2006, **128**, 11385-11390.
74 A. E. Bennett, C. M. Rienstra, M. Auger, K. V. Lakshmi and R. G. Griffin, *J. Chem. Phys.*, 1995, **103**, 6951.
75 S. Hayashi and K. Hayamizu, *Bull. Chem. Soc. Jpn.*, 1991, **64**, 688-690.
76 F. Neese, *Wiley Interdisciplinary Reviews-Computational Molecular Science*, 2012, **2**, 73-78.
77 F. A. Cotton, B. G. de Boer, M. D. Laprade, J. R. Pipal and D. A. Ucko, *Acta Crystallogr., Sect. B: Struct. Sci.*, 1971, **B 27**, 1664-1671.
78 A. D. Becke, *J. Chem. Phys.*, 1993, **98**, 1372-1377.
79 A. D. Becke, *J. Chem. Phys.*, 1993, **98**, 5648-5652.
80 C. T. Lee, W. T. Yang and R. G. Parr, *Phys. Rev. B*, 1988, **37**, 785-789.
81 W. J. Hehre, R. Ditchfield and J. A. Pople, *J. Chem. Phys.*, 1972, **56**, 2257.
82 J. D. Dill and J. A. Pople, *J. Chem. Phys.*, 1975, **62**, 2921-2923.
83 K. A. Peterson, D. Figgen, M. Dolg and H. Stoll, *J. Chem. Phys.*, 2007, **126**.
84 T. Clark, J. Chandrasekhar, G. W. Spitznagel and P. V. Schleyer, *J. Comput. Chem.*, 1983, **4**, 294-301.
85 M. J. Frisch, J. A. Pople and J. S. Binkley, *J. Chem. Phys.*, 1984, **80**, 3265-3269.
86 R. Krishnan, J. S. Binkley, R. Seeger and J. A. Pople, *J. Chem. Phys.*, 1980, **72**, 650-654.

87 S. Abdulhussain, H. Breitzke, T. Ratajczyk, A. Gruenberg, M. Srour, D. Arnaut, H. Weidler, U. Kunz, H. J. Kleebe, U. Bommerich, J. Bernarding, T. Gutmann and G. Buntkowsky, *Chem. - Eur. J.*, 2014, **20**, 1159-1166.
88 V. Schimming, C.-G. Hoelger, G. Buntkowsky, I. Sack, J.-H. Fuhrhop, S. Rocchetti and H. H. Limbach, *J. Am. Chem. Soc.*, 1999, **121**, 4892-4893.
89 O. Lafon, A. S. L. Thankamony, T. Kobayashi, D. Carnevale, V. Vitzthum, I. I. Slowing, K. Kandel, H. Vezin, J. P. Amoureux, G. Bodenhausen and M. Pruski, *J. Phys. Chem. C*, 2013, **117**, 1375-1382.